Applied Catalysis B: Environmental 259 (2019) 118090

Contents lists available at ScienceDirect

Applied Catalysis B: Environmental

journal homepage: www.elsevier.com/locate/apcatb

Engineering oxygen vacancies of cobalt tungstate nanoparticles enable efficient water splitting in alkaline medium

Fang Luo[a,1], Ruizhi Xu[a,1], Shuangxiu Ma[a,1], Quan Zhang[a], Hao Hu[a], Kongang Qu[b], Shenglin Xiao[a], Zehui Yang[a,*], Weiwei Cai[a,*]

[a] Sustainable Energy Laboratory, Faculty of Materials Science and Chemistry, China University of Geosciences, Wuhan, 430074, China
[b] Shandong Provincial Key Laboratory/Collaborative Innovation Center of Chemical Energy Storage & Novel Cell Technology, Liaocheng University, Liaocheng, 252059, China

ARTICLE INFO

Keywords:
Water splitting
Oxygen vacancies
Cobalt tungstate
Hydrogen evolution reaction
Oxygen evolution reaction

ABSTRACT

Development of earth-abundant, efficient and stable electrocatalysts for water splitting is of crucial importance for environmentally friendly energy conversion and storage. Here, we report an oxygen deficient cobalt tungstate nanoparticles with diameter of 8 nm ($CoWO_{4-x}$@C) as efficient bifunctional electrocatalyst for hydrogen evolution reaction (HER) and oxygen reduction reaction (OER), which exhibits comparable HER activity to commercial Pt/C with overpotentials of 32.5 mV and 46.8 mV vs. RHE to deliver current density of 10 mA cm^{-2} in acidic and alkaline mediums, respectively, ascribed to the rich oxygen vacancies facilitating the hydrogen adsorption and its relative recombination, respectively. Additionally, undetectable degradation is observed for $CoWO_{4-x}$@C after 10,000 potential cycles indicating high durability. Meanwhile, $CoWO_{4-x}$@C requires only 295 mV overpotential to deliver 10 mA cm^{-2} in the OER test, which is better than the benchmarking IrO_2 (313 mV). 1.57 V comparably lower than Pt/C-IrO_2 (1.59 V) is required for achieving the water splitting current density of 10 mA cm^{-2} without any degradation for 12 h.

1. Introduction

Hydrogen has been extensively investigated as future energy carrier due to its sustainability, renewability, zero emission and high energy density [1–3]. Growing attention has been paid to the electrochemical or photoelectrochemical water splitting technology for H_2 generation with high purification since water splitting can be driven by the sustainable energies, which is recognized as the environmentally friendly approach for H_2 generation. Generally, water splitting consists of two different redox electrocatalysts to facilitate hydrogen evolution reaction (HER) and oxygen evolution reaction (OER) catalysis, respectively [4–7]. Platinum (Pt) and iridium dioxides (IrO_2) are the state-of-the-art electrocatalysts for HER and OER, respectively, which require low overpotentials to attain high water splitting current density [8–10]. However, Pt and IrO_2 are noble metals with limited reserve hindering its large-scale application in water splitting. Thus, developments in cost-effective HER and OER electrocatalysts with superior activity and stability are crucially important to realize the massive H_2 production at low overpotentials.

Recently, bifunctional electrocatalyst capable of efficiently catalyzing HER and OER is extremely attractive. Heteroatom doped carbon materials have been tremendously researched as bifunctional electrocatalyst for water splitting due to the engineered electronic structures of carbon framework since the introduction of secondary element created active sites for HER and OER ascribed to the re-distributed electrons in the sp^2 conjugated carbon matrix [11–16]. Transition metal phosphides [17–20], carbides [21,22], nitrides [23,24], borides [25,26], sulfides [27,28], selenides [29,30] and oxides [31–33] have also been well investigated as efficient bifunctional electrocatalyst for water splitting. Considerable reactivity toward HER and OER of transition metal oxides (TMOs) was originated from the tremendous vacancies capable of facilitating charge transfer and adjusting the hydrogen adsorption/desorption strength leading to the narrowed bandgaps in electrochemical reactions [34–36]; As a consequence, engineering the oxygen vacancies could effectively boost the intrinsic electrocatalytic activity of TMOs [37]. Heteroatom doping [38,39], and nanostructure adjustment [40–42] have been adopted to successfully tune oxygen vacancies of TMOs inducing more accessible active sites for electrochemical reactions. For further improvement in oxygen vacancies, bimetal oxides, such as $NiCo_2O_4$, [43] $CoMn_2O_4$ [44], $CoFe_2O_4$

* Corresponding authors.
E-mail addresses: yeungzehui@gmail.com (Z. Yang), willcai1985@gmail.com (W. Cai).
[1] These authors contributed equally to this work.

https://doi.org/10.1016/j.apcatb.2019.118090
Received 18 June 2019; Received in revised form 4 August 2019; Accepted 13 August 2019
Available online 14 August 2019

[45] and $CoMoO_4$, [46] have been reported as efficient bifunctional electrocatalysts for water splitting ascribed to the more oxygen vacancies compared to monometallic oxides.

Based on the aforementioned consideration, bimetal oxides with small size could offer more oxygen vacancies due to the high exposed surface and a superior water splitting performance should be reached. Here, we deposited cobalt tungstate ($CoWO_4$) nanoparticles on carbon black via a hydrothermal method and annealed the electrocatalyst with H_2 to create oxygen vacancies ($CoWO_{4-x}$@C). Ascribing to the small size of $CoWO_4$ nanoparticles, high concentration of oxygen vacancies could be obtained after H_2 annealing, which was favorable for the efficient water splitting. HER and OER activities of various $CoWO_{4-x}$@C electrocatalysts with different oxygen vacancies have been systematically investigated. A superior electrocatalyst was obtained with only 1.57 V to achieve water splitting current density of 10 mA cm^{-2} comparably lower than benchmark Pt-IrO_2 requiring 1.59 V, which was one of the most efficient TMOs electrocatalysts for water splitting. Compared to previous reported $CoWO_4$ (~30 nm) as OER/ORR electrocatalyst, [47–50] in this work, oxygen deficient ultrafine $CoWO_{4-x}$ nanoparticle (~8 nm) supported on carbon black has been synthesized. Ascribing to the smaller particle size, tremendous oxygen vacancies and efficient electronic conductivity, boosted electrocatalytic activity could be achieved; moreover, an excellent HER activity was also recorded due to the oxygen vacancies as active sites. To the best of our knowledge, $CoWO_{4-x}$ with such small size has not yet been reported as efficient bifunctional electrocatalyst for water splitting.

2. Experimental section

2.1. Materials

All chemicals were of reagent grade and used as received without further purification. Glucose ($C_6H_{12}O_6$, 99%) was purchased from Innochem. Co. Ltd. Ethyl alcohol, sulfuric acid (H_2SO_4, 98 wt%) and potassium hydroxide (KOH), cobalt acetate ($Co(ac)_2$) and ammonium tungstate ($(NH_4)_{10}W_{12}O_{41}$) were purchased from Sinopharm Chemical Reagent Co. Ltd. Cobalt tungsten oxide ($CoWO_4$, 99%), commercial Pt/C (Pt: 20 wt%), commercial IrO_2, graphite rod (99.9995%), glassy carbon electrode (GCE), saturated calomel electrode (SCE) and Hg/HgO electrode were purchased from Alfa Aesar. Nafion solution was obtained from Sigma-Aldrich. De-ionized water was obtained from an ultra-pure purification system (Milli-Q, resistivity ≥ 18.5 MΩ).

2.2. Synthesis of electrocatalyst

$CoWO_{4-X}$@C electrocatalyst was synthesized as follows: $Co(ac)_2$ (1 g) and $(NH_4)_{10}W_{12}O_{41}$ (1 g) was added to de-ionized water (20 mL) under vigorous magnetic stirring for 10 min to form a uniform suspension and then followed by adding glucose (1 g).The mixture was continuous magnetic stirring at room temperature for 1 h. After transferring the mixture into a Teflon-lined autoclave (50 mL), the autoclave was maintained at 200 °C for 24 h and finally cooled down to room temperature. The product was collected by centrifugation and washed with de-ionized water several times, and then dried at 70 °C for 12 h to obtain $CoWO_4$@C. The precursor was further calcined at 600 °C at a heating ramp rate of 5 °C min^{-1} under H_2 (10 vol% in argon) atmosphere for 0 h, 2 h, 4 h and 6 h, respectively.

2.3. Material characterization

The crystal phase of synthesized powder was identified by X-ray diffraction (XRD, Bruker AXS D8-Focus, Germany) with Cu Kα radiation over the range of 2θ from 10° to 70°. The chemical composition of the samples was obtained by X-ray photoelectron spectrum (XPS, Escalab 250XI, ThermoFisher, USA). The micromorphology of $CoWO_{4-X}$@C powder was observed by means of a high-resolution transmission electron microscopy (HR-TEM, FEI Tecnai G2) equipped with an energy-dispersive X-ray spectroscope (EDS, EDAX Apollo XP, USA).

2.4. Electrochemical measurements

Electrochemical measurements were performed at room temperature using a typical three-electrode system, carried out on Gamry with graphite rod as the counter electrode, SCE and Hg/HgO electrode as the reference electrode in acid and alkaline solutions, respectively. Carbon paper (1 cm × 1 cm) covered with 2 mg of catalyst as the working electrode. Linear scan voltammetry (LSV) at a scan rate of 5 mV s^{-1} was conducted under N_2-saturated 0.5 M H_2SO_4 using SCE, or under N_2-saturated 1 M KOH using Hg/HgO electrode. CV was carried out between 0.16 and 0.26 V vs. RHE at various sweep rates ranging from 10 to 100 mV s^{-1} to investigate the electrochemical double-layer capacitances. The electrochemical impedance spectroscopy (EIS) measurements were performed over the frequency range from 1 MHz to 0.01 Hz with an applied perturbation voltage of 10 mV as the excitation AC amplitude and DC voltage biased at a cathodic overpotential at 10 mA cm^{-2}. Durability of electrocatalyst was carried out by potential cycling from ranging from -0.3 to 0.2 V vs. RHE with scan rate of 50 mV s^{-1}. Oxygen evolution reaction (OER) test was carried out in O_2 purged 1 M KOH electrolyte from 1.2 V to 1.7 V vs. RHE with scan rate of 5 mV s^{-1}. A potential ranging from 1.09 to 1.14 V versus RHE was chosen for the double layer capacitance estimation. Durability test was carried out by potential cycling from 1.2 V to 1.7 V vs. RHE with scan rate of 50 mV s^{-1}. Before the overall water splitting test, the electrolyte was degassed by bubbling pure nitrogen for at least 0.5 h to meet the criteria for practical application. For overall water splitting electrolysis, a two-electrode configuration was used for electrochemical test, where $CoWO_{4-x}$@C electrodes were directly used as both cathode and anode. For comparison, Commercial Pt/C and IrO_2 were used as HER and OER electrocatalysts, respectively.

3. Results and discussion

X-ray diffraction (XRD) pattern of the newly synthesized cobalt tungstate electrocatalyst (denoted as $CoWO_{4-x}$@C-T, T represents the H_2 annealing time) shown in Fig. 1**a** highly matched with the commercial $CoWO_4$ indicating successful formation of $CoWO_4$, in which a sharp peak at 31° was assigned to the dominant (-111) facet of $CoWO_4$ (JCPDS No. 15-0867). Meanwhile, $CoWO_{4-x}$@C-0, $CoWO_{4-x}$@C-2 and $CoWO_{4-x}$@C-6 showed the similar XRD patterns (**Figure S1**) illustrating that H_2 annealing process ineffectively affected the crystal structure of $CoWO_4$. X-ray photoelectron spectroscopy (XPS) was shown in **Figure S2**. Co^{3+}, Co^{2+} and satellite Co species from the deconvoluted Co2p peak were distinctly shown in Fig. 1**b**. Meanwhile, a doublet peak at 35.8 eV and 38 eV assigned to W4f peak was deconvoluted to W^{6+} and W^{5+} species as shown in Fig. 1c, respectively. Similarly, different valences of Co and W species were observed for $CoWO_{4-x}$@C-0 (**Figure S3**), $CoWO_{4-x}$@C-2 (**Figure S4**) and $CoWO_{4-x}$@C-6 (**Figure S5**) electrocatalysts. The quantitative analysis depicted that more Co^{2+} and W^{5+} species were observed with longer H_2 annealing time and became stable after annealing for 4 h as shown in **Table S1**. Co^{2+}/Co^{3+} and W^{5+}/W^{6+} ratios were increased from 1:1 to 1.7:1 and 1.2:1 after H_2 annealing for 4 h, respectively, suggesting that more oxygen vacancies were induced by H_2 annealing process, which were the actual active sites for hydrogen evolution reaction (HER) and oxygen evolution reaction (OER). Consequently, morphology of $CoWO_{4-x}$@C-4 was measured by TEM shown in Fig. 1d, in which $CoWO_{4-x}$ with a diameter of 8 nm were uniformly dispersed on carbon black derived from the carbonization of glucose (**Figure S6**). The fabricated $CoWO_{4-x}$@C-4 electrocatalyst was morphologically different compared to commercial $CoWO_4$ possessing hollow micropores structure shown in **Figure S7a**. From the HR-TEM image (Fig. 1e), a lattice fringe with spacing of 0.29 nm was attributed to the dominant (-111) plane of $CoWO_4$ well

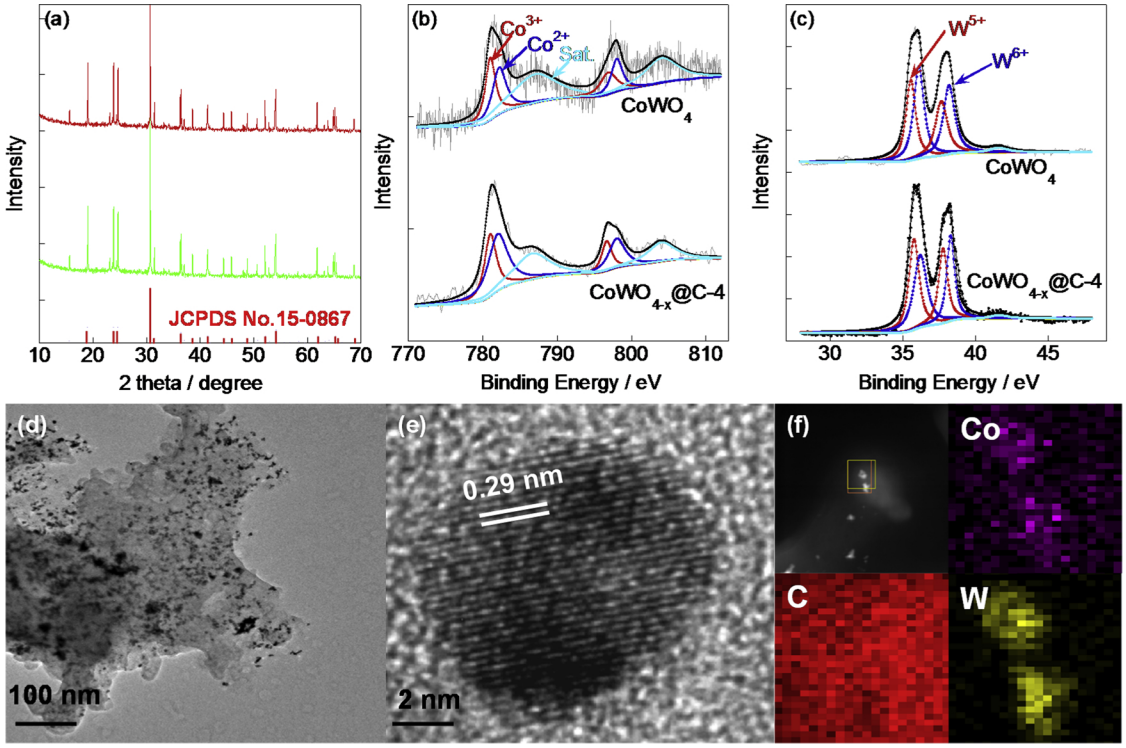

Fig. 1. (a) XRD patterns of commercial $CoWO_4$ (green line) and $CoWO_{4-x}$@C-4 (red line) electrocatalysts. Deconvoluted Co 2p (b) and W 4f (c) peaks of commercial $CoWO_4$ and $CoWO_{4-x}$@C-4 electrocatalysts. TEM (d), HR-TEM (e), HAADF-STEM (f) images and relative EDS mappings of C@$CoWO_{4-x}$@C-4 electrocatalyst.

agreed with the XRD result. The HAADF-STEM image and relative energy dispersive spectrometer (EDS) mappings illustrated the successful formation of $CoWO_{4-x}$@C electrocatalyst (Fig. 1f). Additionally, without H_2 annealing, $CoWO_4$ nanoparticles were still formed and well-anchored on carbon black shown in **Figure S7b**. As shown in **Figure S8**, $CoWO_{4-x}$ content in the electrocatalyst was estimated to 85 wt% by TGA test; thus, the percentage of carbon in all electrocatalysts was 15 wt%.

Hydrogen evolution reaction (HER) test is firstly examined in N_2-

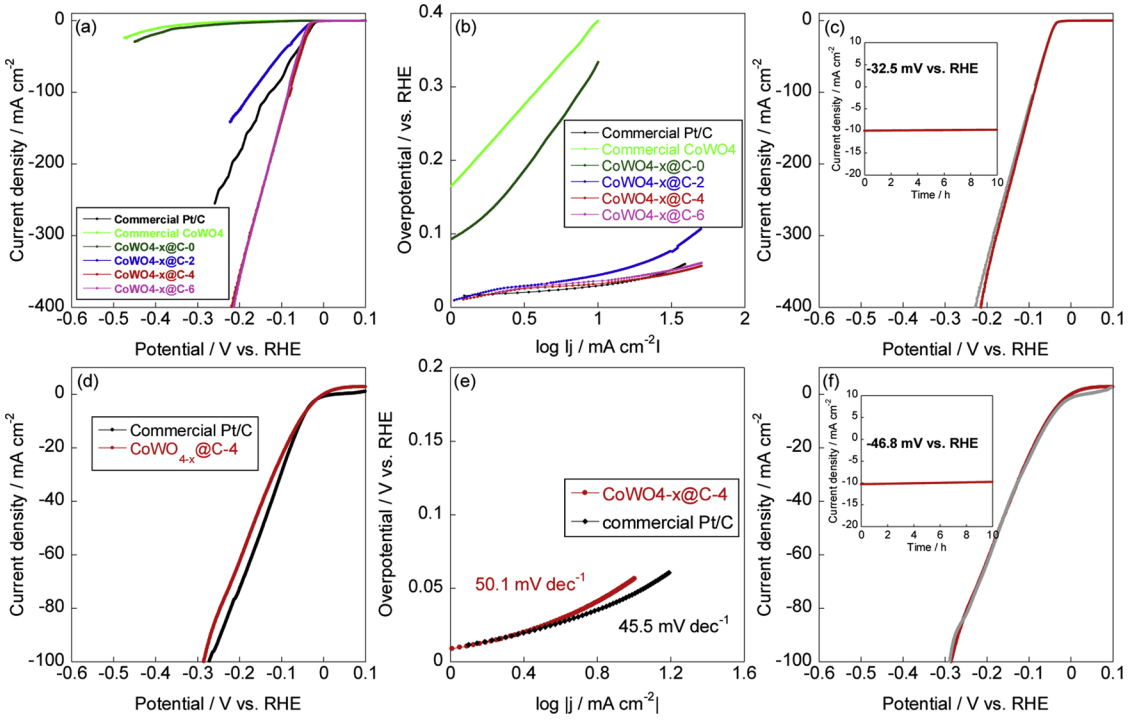

Fig. 2. HER performances (a) and Tafel slopes (b) of commercial Pt/C, commercial $CoWO_4$ and various $CoWO_{4-x}$@C electrocatalysts measured in 0.5 M H_2SO_4 electrolyte. (c) Durability results of $CoWO_{4-x}$@C-4 electrocatalyst tested in 0.5 M H_2SO_4 electrolyte. HER performances (d) and Tafel slopes (e) of commercial Pt/C and $CoWO_{4-x}$@C-4 electrocatalysts recorded in 1 M KOH electrolyte. (f) Durability results of $CoWO_{4-x}$@C-4 electrocatalyst tested in 1 M KOH electrolyte; chronoamperometric stability test was inserted.

purged 0.5 M H_2SO_4 electrolyte shown in Fig. 2**a**. All LSV curves have been iR-corrected to eliminate the impact of the solution resistance. And the reference electrode has been calibrated before testing as shown in **Figure S9**. All the potential was converted to reversible hydrogen electrode based on the equation: E(RHE) = E(SCE) + 0.244 + 0.0591*pH. Ultra-small onsetpotentials (denoted as overpotential@1 mA cm^{-2}) of 11 mV, 10 mV and 10.5 mV vs. RHE were obtained for $CoWO_{4-x}$@C-2, $CoWO_{4-x}$@C-4 and $CoWO_{4-x}$@C-6 electrocatalysts, respectively, both of which were lower compared to the commercial $CoWO_4$ and $CoWO_{4-x}$@C-0 with onsetpotentials of 165 and 93.5 mV vs. HRE. The decreased onsetpotential highlighted that the oxygen vacancies in $CoWO_{4-x}$@C facilitated the adsorption of hydrogen ions (Volmer step: $H_3O^+ + e^- + * \rightarrow *H_{ads} + H_2O$). Additionally, onsetpotentials of all $CoWO_{4-x}$@C electrocatalysts were comparably lower than the benchmark Pt/C requiring 15 mV vs. RHE to deliver catalytic current density of 1 mA cm^{-2}. Overpotentials@10 mA cm^{-2} utilized for the evaluation of HER activity were 333 mV, 45 mV, 32.5 mV and 35.3 mV vs. RHE for $CoWO_4$@C-0, $CoWO_{4-x}$@C-2, $CoWO_{4-x}$@C-4 and $CoWO_{4-x}$@C-6 electrocatalysts, respectively, emphasizing the facilitation of HER by the oxygen vacancies acting as active sites. Besides, more oxygen vacancies were beneficial for the recombination of adsorbed hydrogen atoms to release H_2 molecule. The more oxygen vacancies (active sites) in $CoWO_{4-x}$@C-4 and $CoWO_{4-x}$@C-6 were proved by the electrochemical surface area (ECSA) estimated from double layer capacitances (**Figure S10**). ECSAs of commercial $CoWO_4$, $CoWO_{4-x}$@C-0, $CoWO_{4-x}$@C-2, $CoWO_{4-x}$@C-4 and $CoWO_{4-x}$@C-6 were calculated to 0.29 m F cm^{-2}, 0.31 m F cm^{-2}, 0.88 m F cm^{-2}, 1.59 m F cm^{-2} and 1.58 m F cm^{-2}, respectively, which was consistent with the XPS analysis showing that more oxygen vacancies were created with the increased H_2 annealing time; as a consequence, boosted HER activities were achieved for $CoWO_{4-x}$@C-4 and $CoWO_{4-x}$@C-6 electrocatalysts. $CoWO_{4-x}$@C-4 possessed similar Co^{2+}/Co^{3+} and W^{5+}/W^{6+} ratios to $CoWO_{4-x}$@C-6 resulted in analogous HER activity. Overpotential for delivering catalytic current density above 100 mA cm^{-2} was particularly important for industrial water splitting application to generate massive hydrogen by means of water electrolysis. $CoWO_{4-x}$@C-4 required 218 mV vs. RHE to deliver catalytic current density of 400 mA cm^{-2} outperforming the benchmark Pt/C reaching only 200 mA cm^{-2} at the same overpotential highlighting the better HER activity than Pt/C. Consequently, the HER kinetics of electrocatalyst was studied by Tafel slope extracted from LSV curves shown in Fig. 2**b**. Tafel slopes of commercial $CoWO_4$ and $CoWO_{4-x}$@C-0 were 225.3 mV dec^{-1} and 254.5 mV dec^{-1} ascribed to the less active sites triggering difficulty in adsorption in hydrogen ions ($H_3O^+ + e^- + * \rightarrow H_{ads} + H_2O$). After annealing with H_2, Tafel slopes were decreased to 54.9 mV dec^{-1}, 31.2 mV dec^{-1} and 31.5 mV dec^{-1} for $CoWO_{4-x}$@C-2, $CoWO_{4-x}$@-4 and $CoWO_{4-x}$@C-6 electrocatalysts, respectively due to the more generated active sites for electro-adsorption as well as the desorption of hydrogen atoms. Tafel slopes of $CoWO_{4-x}$@C-4 and $CoWO_{4-x}$@-6 were comparable to commercial Pt/C (30.5 mV dec^{-1}), which was indicative of similar HER kinetics following Volmer-Heyrovsky mechanism. More active sites triggered lower Tafel slope since Heyrovsky reaction ($H_3O^+ + *H_{ads} + e^- \rightarrow H_2 + H_2O + *$) is the rate-determining step (40 mV dec^{-1}) for HER and more active sites increase the possibility of combination of hydrogen atoms to generate H_2 molecule. [51] Due to the rich oxygen vacancies, the hydrogen adsorption strength of $CoWO_4$ was modulated ascribed to the tailored electronic structure. [52] Besides, charge transfer resistance (R_{ct}) is of paramount significance for HER estimated from electrochemical impedance spectroscopy (EIS) shown in **Figure S11**. Due to the presence of carbon black derived from carbonization of glucose, a lower R_{ct} of 13 Ω was obtained for $CoWO_{4-x}$@C-4 compared to commercial $CoWO_4$ (18.5 Ω). Moreover, with increment in annealing time, R_{ct} was decreased to 8 Ω, 3.1 Ω and 3.2 Ω for $CoWO_{4-x}$@C-2, $CoWO_{4-x}$@C-4 and $CoWO_{4-x}$@C-6 electrocatalysts since oxygen vacancies introduced gap states transforming the metal oxides (semiconductor) to degraded one with high conductivity because of the interrupted electron distribution around Fermi level. The low R_{ct} and large ECSA co-contributed to the boosted HER activities of $CoWO_{4-x}$@C-4 and $CoWO_{4-x}$@C-6 electrocatalysts. Co_3O_{4-x}@C (**Figure S12a**) and WO_{3-x}@C (**Figure S12b**) were obtained with only one metal precursor ($Co(ac)_2$ or $(NH_4)_{10}W_{12}O_{41}$) evidenced by the XRD patterns. HER performances of $CoWO_{4-x}$@C-4 and $CoWO_{4-x}$@C-6 outperformed Co_3O_{4-x}@C-4 (overpotential@10 mA cm^{-2}: 188 mV vs. RHE; Tafel slope: 133 mV dec^{-1}) and WO_{3-x}@C-4 (overpotential@10 mA cm^{-2}: 80 mV vs. RHE; Tafel slope: 68.5 mV dec^{-1}) electrocatalysts shown in **Figure S13**, which was due to the synergetic effect favorable for creating more oxygen vacancies in $CoWO_{4-x}$@C electrocatalyst (**Figure S14**). Moreover, $CoWO_{4-x}$@C-4 was recognized one of the most efficient HER electrocatalysts among the recently reported TMOs as shown in **Table S2**. In order to verify the importance of carbon in the electrocatalyst, $CoWO_{4-x}$ was prepared without glucose and $CoWO_{4-x}$ required overpotential of 132 mV vs. RHE to deliver 10 mA cm^{-2} (**Figure S15a**), which exhibited much lower HER performance than $CoWO_{4-x}$@C-4 due to the lower ECSA of $CoWO_{4-x}$ (0.46 m F cm^{-2}, **Figure S15b**) and higher R_{ct} (5.3 Ω, **Figure S15d**). The lower HER activity of $CoWO_{4-x}$ depicted the importance of carbon, which was favorable for uniform dispersion of $CoWO_{4-x}$ and electron transfer. A comparable HER activity was recorded for $CoWO_{4-x}$@C-4 and $CoWO_{4-x}$@C-6 depicting that annealing with H_2 for 4 h was enough to obtain sufficient oxygen vacancies for efficient HER catalysis. Thus, $CoWO_{4-x}$@C-4 was chosen for durability and stability evaluation, which are crucial factors for HER electrocatalyst. As shown in Fig. 2c, undetectable increment in overpotential for attaining 10 mA cm^{-2} was observed after 10,000 potential cycles and only 14 mV positive shift was obtained for reaching catalytic current density of 400 mA cm^{-2} attributed to the small loss in ECSA from 1.59 m F cm^{-2} to 1.37 m F cm^{-2} and unchanged R_{ct} (3.1 Ω) after durability test as shown in **Figure S16**. In contrast, benchmark Pt/C exhibited a serious deterioration in HER performance with overpotentials for 10 mA cm^{-2} and 200 mA cm^{-2} increased from 30 mV and 218 mV vs. RHE to 40 mV and 344 mV vs. RHE (**Figure S17a**) due to the loss of active sites represented by the decreased ECSA calculated from hydrogen adsorption peak (**Figure S17b**). After durability test, the electrocatalyst was measured by TEM shown in **Figure S18a**, in which $CoWO_{4-x}$ nanoparticles were still homogenously dispersed on carbon black with a diameter of 8 nm and lattice fringe with spacing of 0.29 nm corresponding to the (-111) facet of $CoWO_{4-x}$ (**Figure S18b**) confirmed the stable structure of $CoWO_{4-x}$ nanoparticles during durability test, which was consistent with XPS test shown in **Figure S19**. The quantitative analysis of $CoWO_{4-x}$@C-4 electrocatalyst suggested that similar Co^{2+}/Co^{3+} and W^{5+}/W^{6+} ratios were obtained before and after durability test (**Table S1**) indicating that oxygen vacancies were stable during the durability test contributing to the stable HER activity. Furthermore, almost no degradation in current density was recorded for 10 h suggesting high chronoamperometric stability. Continuously, HER performance of $CoWO_{4-x}$@C-4 was further tested in N_2 deoxygenated 1 M KOH electrolyte shown in Fig. 2d, in which a comparable overpotential@10 mA cm^{-2} of 46.8 mV vs. RHE was obtained for $CoWO_{4-x}$@C-4 to that of benchmark Pt/C requiring 46.4 mV overpotential to deliver 10 mA cm^{-2}. Moreover, $CoWO_{4-x}$@C-4 and Pt/C required similar overpotentials to reach 100 mA cm^{-2} in 1 M KOH electrolyte. The Tafel slope of $CoWO_{4-x}$@C-4 was 50.1 mV dec^{-1} comparable to that of Pt/C (45.5 mV dec^{-1}, Fig. 2e) illustrating that $CoWO_{4-x}$@C-4 followed Volmer-Heyrovsky HER mechanism similar to benchmark Pt/C. Consequently, durability of $CoWO_{4-x}$@C-4 was investigated and almost no degradation in HER activity after 10,000 potential cycles (Fig. 2f) due to the similar ECSAs (before: 1.71 m F cm^{-2}, after: 1.59 m F cm^{-2}) calculated from double-layer capacitance and ignorable increment in R_{ct} (before: 3.8 Ω, after: 4.4 Ω) during the durability test (**Figure S20**). The HER performance of benchmark Pt/C was decreased after only 2000 potential cycles with overpotential@10 mA cm^{-2} increased from 46.8 mV to 66 mV vs. RHE (**Figure S21**). Electrocatalytic current density of 10 mA cm^{-2} was stably recorded for 10 h with applied potential of 46.8 mV vs. RHE, which was a strong

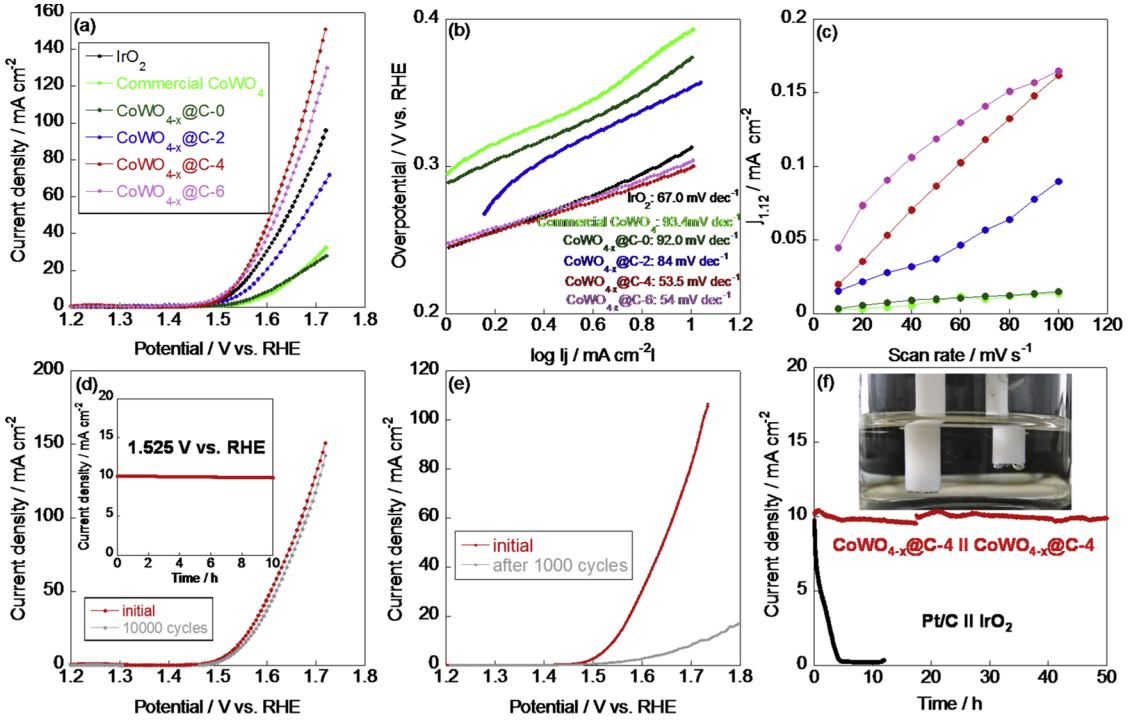

Fig. 3. (a) Oxygen evolution reaction (OER) curves, Tafel slopes (b) and double layer capacitances (c) of commercial IrO_2, commercial $CoWO_4$ and various $CoWO_{4-x}$@C electrocatalysts recorded in 1 M KOH electrolyte. OER curves of $CoWO_{4-x}$@C-4 (d) and commercial IrO_2 (e) electrocatalysts before (red line) and after (grey line) durability test. (f) Stability test of water splitting test fabricated from $CoWO_{4-x}$@C-4 (red line) and Pt/C-IrO_2 (black line) for 50 h.

indication of high durability and $CoWO_{4-x}$@C-4 could potentially replace Pt/C as cathodic electrocatalyst for the industrial water splitting. Not surprisingly, $CoWO_{4-x}$ nanoparticles were still uniformly dispersed on carbon black and lattice fringe with spacing of 0.29 nm was still observed attributed to the (-111) facet of $CoWO_{4-x}$ (**Figure S22**). Moreover, XPS test indicated that the oxygen vacancies were also stable during the durability test (**Figure S23**).

Electrocatalytic activity toward oxygen evolution reaction (OER) is evaluated in O_2 purged 1 M KOH electrolyte shown in Fig. 3**a**. Benchmark IrO_2 electrocatalyst with overpotential@10 mA cm^{-2} of 313 mV vs. RHE (Fig. 3a) and Tafel slope of 67 mV dec^{-1} (Fig. 3b) was recorded, which was in good agreement with previous reports. Overpotentials@ 10 mA cm^{-2} were 374 mV, 354 mV, 295 mV and 304 mV vs. RHE for $CoWO_{4-x}$@C-0, $CoWO_{4-x}$@C-2, $CoWO_{4-x}$@C-4 and $CoWO_{4-x}$@C-6 electrocatalysts, respectively. The boosted OER activity was due to the more oxygen vacancies induced by H_2 annealing since these oxygen vacancies facilitated the adsorption of OH- species as well as the discharge process of adsorbed OH- species. [16,53,54] Meanwhile, the Tafel slope was decreased from 92 mV dec^{-1} to 54 mV dec^{-1} after H_2 annealing due to the large ECSA (commercial $CoWO_4$: 0.13 m F cm^{-2}; $CoWO_{4-x}$@C-0: 0.12 m F cm^{-2}; $CoWO_{4-x}$@C-2: 0.8 m F cm^{-2}; $CoWO_{4-x}$@C-4: 1.58 m F cm^{-2} and $CoWO_{4-x}$@C-6: 1.45 m F cm^{-2}, Fig. 3c) estimated from double layer capacitances (**Figure S24**) and low R_{ct} ($CoWO_{4-x}$@C-0: 4.5 Ω; $CoWO_{4-x}$@C-2: 3.3 Ω; $CoWO_{4-x}$@C-4: 3.0 Ω and $CoWO_{4-x}$@C-6: 2.9 Ω, **Figure S25**). $CoWO_{4-x}$@C-4 required only 458 mV vs. RHE overpotential to reach 100 mA cm^{-2}, which was particularly low compared to commercial IrO_2 electrocatalyst (494 mV vs. RHE). Additionally, $CoWO_{4-x}$@C-4 exhibited better OER performance than those of Co_3O_{4-x}@C-4 (overpotential@10 mA cm^{-2}: 363 mV vs. HRE; Tafel slope: 70.1 mV dec^{-1}) and WO_{3-x}@C-4 (overpotential@10 mA cm^{-2}: 428 mV vs. HRE; Tafel slope: 102.3 mV dec^{-1}, **Figure S26**) electrocatalysts ascribed to the more oxygen vacancies resulting in more active sites similar to HER test. Subsequently, durability test was carried out and overpotential@10 mA cm^{-2} was only increased by 6 mV after 10,000 potential cycles (Fig. 3d) due to the slightly decreased ECSA (before: 1.58 m F cm^{-2}; after: 1.35 m F cm^{-2}, **Figure S27**) calculated from double-layer capacitance. Also, the R_{ct} was only increased from 3.0 Ω to 4.5 Ω after durability test. Stable structure was confirmed by the HR-TEM and HAADF-STEM tests after durability evaluation (**Figure S28**). Moreover, oxygen vacancies in $CoWO_{4-x}$@C-4 were almost similar to the initial value proved by the quantitatively analyzed XPS test shown in **Figure S29**. Comparatively, commercial IrO_2 showed a sharp degradation in OER activity after merely 1000 potential cycles (Fig. 3e) due to the loss in ECSA (**Figure S30**). Additionally, a stable catalysis current density of 10 mA cm^{-2} was recorded for 10 h at overpotential of 295 mV vs. RHE. Thus, $CoWO_{4-x}$@C-4 could be potentially utilized as alternative OER electrocatalyst in alkaline water splitting. Finally, the water splitting test was carried out by two-electrode system in 1 M KOH. Pt/C-IrO_2 based water splitting device required a cell voltage of 1.59 V to attain current density of 10 mA cm^{-2} and current density was sharply decreased to almost 0 mA cm^{-2} after 4 h; while, 1.57 V was required to achieve 10 mA cm^{-2} for $CoWO_{4-x}$@C-4 and 9.6 mA cm^{-2} was still remained after water splitting for 50 h. After water splitting test, the HER and OER performances of $CoWO_{4-x}$@C-4 electrocatalyst were measured and negligible degradation in HER (**Figure S31**) and OER (**Figure S32**) activities were recorded highlighting the exceptional stability. Thus, $CoWO_{4-x}$@C-4 with rich oxygen vacancies was efficient and stable bifunctional electrocatalyst for water splitting.

DFT calculation results of HER reaction pathways (Volmer-Heyrovsky mechanism) for $CoWO_4$ (**Figure S33**) and $CoWO_{4-x}$ (**Figure S34**) were displayed in Fig. 4**a**. In acidic condition, the reaction pathway mainly included H_3O^+ adsorption and reduction on the surface to form absorbed hydrogen atoms on the active sites, which were the top-W site of $CoWO_{4-x}$ and top-O site of $CoWO_4$ (Fig. 4b). For $CoWO_{4-x}$, the exterior W^{5+} species were of great significance for the adsorption and relative desorption of those intermediates. W^{5+} anions were able to donate electrons to form W^{6+} species and then recovered by accepting electrons. The charge balance was maintained by the W^{5+}/W^{6+} pairs, the cooperation between the W^{5+} and oxygen vacancies can ameliorate the HER process; while, in case of $CoWO_4$, the

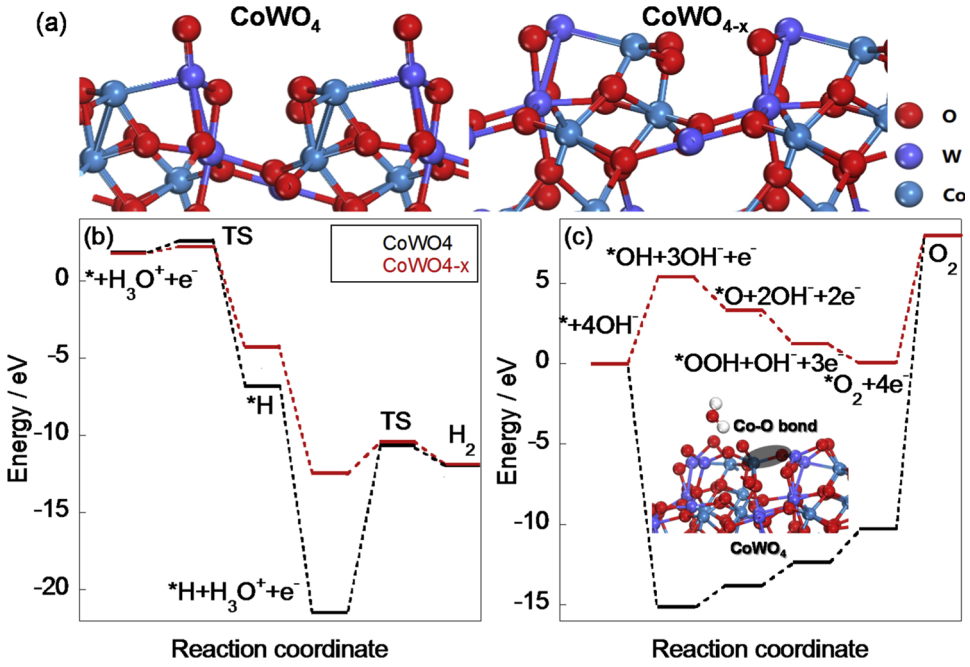

Fig. 4. Structures of (-111) facet of $CoWO_4$ and $CoWO_{4-x}$. Calculated free energies of $CoWO_4$ and $CoWO_{4-x}$ during HER (b) and OER (c).

strong absorption of H_{ads} could retard the formation of the H_2. Besides, the transition state (TS) of the H_2 formation of $CoWO_4$ was 10.08 eV, which was significantly higher than the barrier of $CoWO_{4-x}$ (1.86 eV) revealing that it was difficult for the HER process to procedure on the $CoWO_4$ surface with no oxygen vacancies similar to experimental results (Fig. 2a). Normally, the HER performance in acidic medium exhibited similar trend to HER activity in alkaline; thus, better HER activity in alkaline electrolyte was expected for $CoWO_{4-x}$. Consequently, the OER was calculated based on the discharge process of $4OH^-$ species for $CoWO_4$ (**Figure S35**) and $CoWO_{4-x}$ (**Figure S36**). Through the DFT calculation, we noted that the absorption energy of the formation of OH_{ads} species on $CoWO_{4-x}$ is 5.40 eV and a significant energy drop of -15.11 eV was observed for $CoWO_4$ (Fig. 4c). Unlike $CoWO_{4-x}$, in the absorption process of $CoWO_4$, extra Co-O bonds were formed. In addition, the OH^- underwent a diffusion process and formed a new O—H bond with the O atom on the surface. The formation of extra bond on the surface of $CoWO_4$ led to a significant energy drop of the absorption process resulted in the difficulty of desorption process afterwards. The formation of extra Co-O bonds stabilized the O_{ads} specie making it difficult to release O_2 molecule (18.24 eV). In comparison, the oxygen defect $CoWO_{4-x}$ created W or Co sites for the reaction and stabilized the unpaired electron of O atoms and assisted in the formation of O—O coupling leading to a moderate barrier of O_{ads} formation and O_2 release (7.98 eV). [55] The DFT calculation highlighted the importance of oxygen vacancies in $CoWO_4$ for boosting HER and OER activities.

4. Conclusions

In summary, oxygen defect $CoWO_{4-x}$ nanoparticles with a diameter of 8 nm were deposited on carbon black ($CoWO_{4-x}$@C). Due to the rich oxygen vacancies, $CoWO_{4-x}$@C performed remarkable HER activity with overpotentials of 32.5 mV and 46.8 mV vs. RHE to deliver cathodic current density of 10 mA cm^{-2} in 0.5 M H_2SO_4 and 1 M KOH electrolyte, respectively. Moreover, OER performance of $CoWO_{4-x}$@C with overpotential of 295 mV vs. RHE to achieve 10 mA cm^{-2} outperformed the benchmarking IrO_2 in 1 M KOH electrolyte. Consequently, only 1.57 V was required for reaching 10 mA cm^{-2} in alkaline water splitting application, which was lower than Pt-IrO_2 demanding 1.59 V. Additionally, $CoWO_{4-x}$@C electrocatalyst exhibited exceptionally stability highlighting its potential application in alkaline water splitting.

Declaration of Competing Interest

The authors declare that they have no known competing financial interests or personal relationships that could have appeared to influence the work reported in this paper.

Acknowledgements

This work is supported by the National Natural Science Foundation of China (Nos. 21703212, 21875224). Fang Luo also acknowledged the Fundamental Research Funds for National Universities, China University of Geosciences (Wuhan).

Appendix A. Supplementary data

Supplementary material related to this article can be found, in the online version, at doi:https://doi.org/10.1016/j.apcatb.2019.118090.

References

[1] X. Zou, Y. Zhang, Chem. Soc. Rev. 44 (2015) 5148–5180.
[2] C. Du, L. Yang, F. Yang, G. Cheng, W. Luo, ACS Catal. 7 (2017) 4131–4137.
[3] K. Li, J. Zhang, R. Wu, Y. Yu, B. Zhang, Adv. Sci. 3 (2016) 1500426.
[4] Y. Lyu, R. Wang, L. Tao, Y. Zou, H. Zhou, T. Liu, Y. Zhou, J. Huo, S.P. Jiang, J. Zheng, S. Wang, Appl. Catal. B 248 (2019) 277–285.
[5] D. Yan, R. Chen, Z. Xiao, S. Wang, Electrochim. Acta 303 (2019) 316–322.
[6] Y. Zou, Z. Liu, R. Liu, D. Liu, C. Dong, Y. Wang, S. Wang, J. Power Sources 427 (2019) 215–222.
[7] P. Zhou, J. He, Y. Zou, Y. Wang, C. Xie, R. Chen, S. Zang, S. Wang, Sci. China Chem. (2019).
[8] F. Luo, Q. Zhang, X. Yu, S. Xiao, Y. Ling, H. Hu, L. Guo, Z. Yang, L. Huang, W. Cai, H. Cheng, Angew. Chem. Int. Ed. 57 (2018) 14862–14867.
[9] F.-X. Ma, H.B. Wu, B.Y. Xia, C.-Y. Xu, X.W. Lou, Angew. Chem. Int. Ed. 127 (2015) 15615–15619.
[10] Y. Ling, Z. Yang, Q. Zhang, Y. Zhang, W. Cai, H. Cheng, Chem. Commun. (Camb.) 54 (2018) 2631–2634.
[11] Y. Xu, M. Kraft, R. Xu, Chem. Soc. Rev. 45 (2016) 3039–3052.
[12] X. Wang, A. Vasileff, Y. Jiao, Y. Zheng, S.-Z. Qiao, Adv. Mater. 0 1803625.
[13] M.-S. Balogun, W. Qiu, H. Yang, W. Fan, Y. Huang, P. Fang, G. Li, H. Ji, Y. Tong, Energy Environ. Sci. 9 (2016) 3411–3416.
[14] Z. Zhang, Z. Yi, J. Wang, X. Tian, P. Xu, G. Shi, S. Wang, J. Mater. Chem. A Mater.

Energy Sustain. 5 (2017) 17064–17072.
[15] C. Zhu, M. Zhu, Y. Sun, Y. Zhou, H. Huang, Y. Lifshitz, S.-T. Lee, J. Zhong, Y. Liu, Z. Kang, Appl. Catal. B 237 (2018) 166–174.
[16] D. Yan, Y. Li, J. Huo, R. Chen, L. Dai, S. Wang, Adv. Mater. 29 (2017) 1606459.
[17] L. Ma, W. Zhang, P. Zhao, J. Liang, Y. Hu, G. Zhu, R. Chen, Z. Tie, J. Liu, Z. Jin, J. Mater. Chem. A Mater. Energy Sustain. 6 (2018) 20076–20082.
[18] J. Luo, H. Wang, G. Su, Y. Tang, H. Liu, F. Tian, D. Li, J. Mater. Chem. A Mater. Energy Sustain. 5 (2017) 14865–14872.
[19] Y. Wang, B. Kong, D. Zhao, H. Wang, C. Selomulya, Nano Today 15 (2017) 26–55.
[20] F. Yu, H. Zhou, Y. Huang, J. Sun, F. Qin, J. Bao, W.A. Goddard, S. Chen, Z. Ren, Nat. Commun. 9 (2018) 2551.
[21] N. Han, K.R. Yang, Z. Lu, Y. Li, W. Xu, T. Gao, Z. Cai, Y. Zhang, V.S. Batista, W. Liu, X. Sun, Nat. Commun. 9 (2018) 924.
[22] A.T. Garcia-Esparza, D. Cha, Y. Ou, J. Kubota, K. Domen, K. Takanabe, ChemSusChem 6 (2013) 168–181.
[23] N. Han, P. Liu, J. Jiang, L. Ai, Z. Shao, S. Liu, J. Mater. Chem. A Mater. Energy Sustain. 6 (2018) 19912–19933.
[24] S. Dutta, A. Indra, Y. Feng, H. Han, T. Song, Appl. Catal. B 241 (2019) 521–527.
[25] L. Li, Z. Deng, L. Yu, Z. Lin, W. Wang, G. Yang, Nano Energy 27 (2016) 103–113.
[26] N. Xu, G. Cao, Z. Chen, Q. Kang, H. Dai, P. Wang, J. Mater. Chem. A Mater. Energy Sustain. 5 (2017) 12379–12384.
[27] H. Li, S. Chen, Y. Zhang, Q. Zhang, X. Jia, Q. Zhang, L. Gu, X. Sun, L. Song, X. Wang, Nat. Commun. 9 (2018) 2452.
[28] J. Yu, G. Cheng, W. Luo, J. Mater. Chem. A Mater. Energy Sustain. 5 (2017) 15838–15844.
[29] X. Xu, P. Du, Z. Chen, M. Huang, J. Mater. Chem. A Mater. Energy Sustain. 4 (2016) 10933–10939.
[30] C. Panda, P.W. Menezes, C. Walter, S. Yao, M.E. Miehlich, V. Gutkin, K. Meyer, M. Driess, Angew. Chem. Int. Ed. 56 (2017) 10506–10510.
[31] X. Yan, L. Tian, K. Li, S. Atkins, H. Zhao, J. Murowchick, L. Liu, X. Chen, Adv. Mater. Interfaces 3 (2016) 1600368.
[32] H. Xu, R.Q. Zhang, A.M.C. Ng, A.B. Djurišić, H.T. Chan, W.K. Chan, S.Y. Tong, J. Phys. Chem. C 115 (2011) 19710–19715.
[33] Y. Zhao, C. Chang, F. Teng, Y. Zhao, G. Chen, R. Shi, G.I.N. Waterhouse, W. Huang, T. Zhang, Adv. Energy Mater. 7 (2017) 1700005.
[34] F. Cheng, J. Shen, B. Peng, Y. Pan, Z. Tao, J. Chen, Nat. Chem. 3 (2010) 79.
[35] T. Zheng, W. Sang, Z. He, Q. Wei, B. Chen, H. Li, C. Cao, R. Huang, X. Yan, B. Pan, S. Zhou, J. Zeng, Nano Lett. 17 (2017) 7968–7973.
[36] N. Zhang, X. Li, H. Ye, S. Chen, H. Ju, D. Liu, Y. Lin, W. Ye, C. Wang, Q. Xu, J. Zhu, L. Song, J. Jiang, Y. Xiong, J. Am. Chem. Soc. 138 (2016) 8928–8935.
[37] L. Xu, Q. Jiang, Z. Xiao, X. Li, J. Huo, S. Wang, L. Dai, Angew. Chem. Int. Ed. 55 (2016) 5277–5281.
[38] J. Hou, Y. Sun, Y. Wu, S. Cao, L. Sun, Adv. Funct. Mater. 28 (2018) 1704447.
[39] X. Gao, H. Zhang, Q. Li, X. Yu, Z. Hong, X. Zhang, C. Liang, Z. Lin, Angew. Chem. Int. Ed. 128 (2016) 6398–6402.
[40] Y. Jin, H. Wang, J. Li, X. Yue, Y. Han, P.K. Shen, Y. Cui, Adv. Mater. 28 (2016) 3785–3790.
[41] C. Shu, S. Kang, Y. Jin, X. Yue, P.K. Shen, J. Mater. Chem. A Mater. Energy Sustain. 5 (2017) 9655–9660.
[42] Z. Luo, R. Miao, T.D. Huan, I.M. Mosa, A.S. Poyraz, W. Zhong, J.E. Cloud, D.A. Kriz, S. Thanneeru, J. He, Y. Zhang, R. Ramprasad, S.L. Suib, Adv. Energy Mater. 6 (2016) 1600528.
[43] C. Zhu, S. Fu, D. Du, Y. Lin, Chem. Eur. J. 22 (2016) 4000–4007.
[44] S. Peng, F. Gong, L. Li, D. Yu, D. Ji, T. Zhang, Z. Hu, Z. Zhang, S. Chou, Y. Du, S. Ramakrishna, J. Am. Chem. Soc. 140 (2018) 13644–13653.
[45] Y. Ding, J. Zhao, W. Zhang, J. Zhang, X. Chen, F. Yang, X. Zhang, ACS Appl. Energy Mater. (2018).
[46] X. Yan, L. Tian, S. Atkins, Y. Liu, J. Murowchick, X. Chen, ACS Sustain. Chem. Eng. 4 (2016) 3743–3749.
[47] V.K.V.P. Srirapu, A. Kumar, P. Srivastava, R.N. Singh, A.S.K. Sinha, Electrochim. Acta 209 (2016) 75–84.
[48] H. Jia, J. Stark, L.Q. Zhou, C. Ling, T. Sekito, Z. Markin, RSC Adv. 2 (2012) 10874–10881.
[49] C. Ling, L.Q. Zhou, H. Jia, RSC Adv. 4 (2014) 24692–24697.
[50] Saad M. AlShehri, J. Ahmed, T. Ahamad, P. Arunachalam, T. Ahmad, A. Khan, RSC Adv. 7 (2017) 45615–45623.
[51] Y. Li, H. Wang, L. Xie, Y. Liang, G. Hong, H. Dai, J. Am. Chem. Soc. 133 (2011) 7296–7299.
[52] Y.H. Li, P.F. Liu, L.F. Pan, H.F. Wang, Z.Z. Yang, L.R. Zheng, P. Hu, H.J. Zhao, L. Gu, H.G. Yang, Nat. Commun. 6 (2015) 8064-8064.
[53] T. Liu, Z. Feng, Q. Li, J. Yang, C. Li, M. Dupuis, Chem. Mater. 30 (2018) 7714–7726.
[54] Y. Zhu, X. Liu, S. Jin, H. Chen, W. Lee, M. Liu, Y. Chen, J. Mater. Chem. A Mater. Energy Sustain. 7 (2019) 5875–5897.
[55] J. Yan, L. Kong, Y. Ji, J. White, Y. Li, J. Zhang, P. An, S. Liu, S.-T. Lee, T. Ma, Nat. Commun. 10 (2019) 2149-2149.